

# The high temperature creep deformation of $\text{Si}_3\text{N}_4\text{-6Y}_2\text{O}_3\text{-2Al}_2\text{O}_3$

J. A. TODD\*, ZHI-YUE XU†

\*Departments of Materials Science and Mechanical Engineering,  
University of Southern California, Los Angeles, California 90089-0241, USA

†Department of Materials Science, University of Southern California, Los Angeles,  
California 90089-0241, USA

The creep properties of silicon nitride containing 6 wt% yttria and 2 wt% alumina have been determined in the temperature range 1573 to 1673 K. The stress exponent,  $n$ , in the equation  $\dot{\epsilon} \propto \sigma^n$ , was determined to be  $2.00 \pm 0.15$  and the true activation energy was found to be  $692 \pm 25 \text{ kJ mol}^{-1}$ . Transmission electron microscopy studies showed that deformation occurred in the grain boundary glassy phase accompanied by microcrack formation and cavitation. The steady state creep results are consistent with a diffusion controlled creep mechanism involving nitrogen diffusion through the grain boundary glassy phase.

## 1. Introduction

Advanced processing techniques, such as sintering, gas-pressure sintering, post-sintering and hot isostatic pressing (HIP) are currently being developed to improve the mechanical properties of dense silicon nitride ( $\text{Si}_3\text{N}_4$ ) [1]. Achievement of full density in both sintered silicon nitride (SSN) and hot isostatically pressed silicon nitride (HIPSIN) requires the presence of additives to promote densification by liquid phase sintering [2-4]. Three groups of additives have been used [1, 5-7]: (a) oxides ( $\text{MgO}$ ,  $\text{Y}_2\text{O}_3$ ,  $\text{Y}_2\text{O}_3 + \text{Al}_2\text{O}_3$ ), which do not form solid solutions with  $\text{Si}_3\text{N}_4$ ; (b) oxide and non-oxide additives ( $\text{BeO}$ ,  $\text{BeSiN}_2$ ,  $\text{Al}_2\text{O}_3 + \text{AlN}$ ,  $\text{AlN} + \text{Y}_2\text{O}_3$ ) which do form solid solutions with  $\text{Si}_3\text{N}_4$ ; and (c) non-oxide additives ( $\text{Be}_3\text{N}_2$ ,  $\text{ZrN}$ ,  $\text{ZrC}$ ,  $\text{Zr} + \text{AlN}$ ,  $\text{Mg}_3\text{N}_2$ ) which give higher viscosity grain boundary phases. Additives such as  $\text{MgO}$  result in a continuous, amorphous, magnesium silicate intergranular phase [8-11], whilst those containing  $\text{Y}_2\text{O}_3\text{-Al}_2\text{O}_3$  additions may possess both crystalline and amorphous grain boundary phases [12-15]. The presence of a glassy grain boundary phase is deleterious to both the room temperature and elevated temperature mechanical properties of silicon nitride.

The creep properties of dense silicon nitride, which are mainly controlled by grain boundary sliding along the amorphous phase, can be improved by: (1) increasing the viscosity of the grain boundary phase; (2) crystallization of the grain boundary phase; and (3) production of high aspect ratio  $\beta\text{-Si}_3\text{N}_4$  grains, favoured by high viscosity melts [1, 16-19]. Hence, additives such as  $\text{Y}_2\text{O}_3$ , which give a higher viscosity grain boundary phase, generally result in lower creep rates than for  $\text{MgO}$ -doped silicon nitride [20]. However, a second oxide additive,  $\text{Al}_2\text{O}_3$ , is frequently combined with  $\text{Y}_2\text{O}_3$ , to avoid problems of reduced densification rates and higher densification tempera-

tures, produced by the single refractory oxide additive [21, 22].

To date, there have been few reports of the elevated temperature properties of silicon nitride containing refractory and rare-earth oxides [1, 19, 20, 23-26]. The present study was, therefore, undertaken to investigate (a) the creep behaviour of  $\text{Si}_3\text{N}_4\text{-6Y}_2\text{O}_3\text{-2Al}_2\text{O}_3$  (wt %) processed by a two-stage gas-pressure sintering technique; (b) the role of the grain boundary phase; and (c) the rate controlling mechanism for steady state creep.

## 2. Experimental procedures

The material used in this study contained 92 wt % GTE SN 502 powder, 6 wt % Molycorp  $\text{Y}_2\text{O}_3$  powder and 2 wt % Linde  $\text{Al}_2\text{O}_3$  powder, all less than  $1 \mu\text{m}$  in size. The powders were dry-ball milled for 24 h using sintered  $\text{Si}_3\text{N}_4$  grinding media, then blended with a binder, pelletized and injection moulded into test bars  $50.8 \text{ mm} \times 6.4 \text{ mm} \times 3.2 \text{ mm}$ . Following binder burn-out, the specimens were sintered using a two-stage gas pressure sintering technique. The pre-sintering stage, conducted at a nitrogen pressure of 0.6 MPa (90 ksi) for 4 h at 2123 K, was required to remove open porosity. In the second stage, the temperature and pressure were raised to 2173 K and 10.3 MPa (1500 psi) nitrogen for 2 h to complete the densification cycle. (It should be noted that sintering temperatures are limited to 2093 K with 0.1 MPa (atmospheric pressure) nitrogen. The use of higher nitrogen pressures permits sintering at higher temperatures (up to 2473 K for 10 MPa  $\text{N}_2$ ) and the use of smaller quantities of refractory additives.)

Specimens for creep testing were nominally  $25 \text{ mm} \times 3 \text{ mm} \times 3 \text{ mm}$ . They were deformed in four-point flexure with an outer span of 19 mm and an inner span of 6.4 mm. High purity sapphire rods were used for pivot points. The displacement of the inner pivot points was monitored with a linear variable differential transformer and chart recorder. Tests were conducted

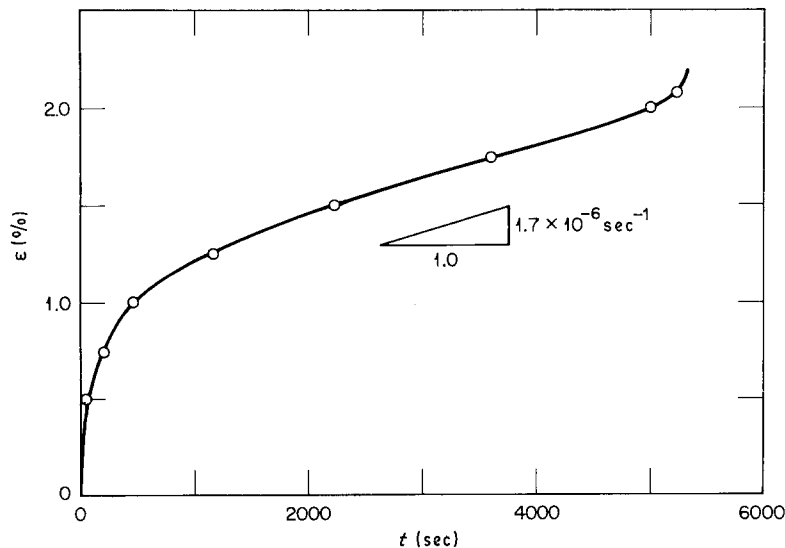


Figure 1 The variation of creep strain,  $\epsilon$  (%) with time,  $t$ , for  $\text{Si}_3\text{N}_4\text{-6Y}_2\text{O}_3\text{-2Al}_2\text{O}_3$  tested at 1673 K and an applied stress of 36.4 MPa.

in an air environment at constant stresses between 10.4 and 52 MPa in the temperature range 1573 to 1673 K. The furnace was allowed to stabilize for 90 min at the test temperature before commencing the creep tests. Stress and strain data were computed for the four-point bend specimen from the load-displacement data using the procedure developed by Hollenberg *et al.* [27].

Scanning electron micrographs were taken from both the polished and etched tensile surfaces and the fracture surfaces of the creep tested samples. Transmission electron microscopy samples were taken from the as-received material and the tensile face of partially deformed creep specimens. The samples were thinned by ion beam milling and examined in a Philips 430 transmission electron microscope operated at 300 kV.

### 3. Results

#### 3.1. Creep data

Creep strain (%) against time data, showing normal primary, secondary and tertiary regions are shown in Fig. 1 for a sample tested at 1673 K and a stress of 36.4 MPa. Strain rate data against strain are summarized in Fig. 2 for specimens tested at 1673 K and stresses in the range 10.4 to 52 MPa. A well defined steady state region was observed for strains above 1%, at all stresses above 19.9 MPa. However, at 10.4 MPa the strain rate continued to decrease with increasing strain and steady state behaviour was not observed. It should be noted that rupture times of 0.4 to 1.2 h and 1.5 to 5.3 h were observed for specimens tested at 52 and 36.1 MPa, respectively, whereas for 19.9 and 10.4 MPa the tests were stopped, prior to rupture, after approximately 22 h.

#### 3.2. Stress exponent

Steady state strain rate data are plotted against stress, for temperatures of 1673, 1623 and 1573 K, in Fig. 3. The error bars for the stress, 10.4 MPa, at 1673 K indicate the strain rates between a strain level of 1.5% and the strain level corresponding to the end of the test. Inspection of Fig. 3 reveals that the creep behaviour of  $\text{Si}_3\text{N}_4\text{-6Y}_2\text{O}_3\text{-2Al}_2\text{O}_3$  is associated with a stress exponent of  $2.00 \pm 0.15$ .

#### 3.3. Activation energy for creep deformation

The apparent activation energy for creep deformation was determined from the secondary creep rate against applied stress data shown in Fig. 3, for an applied stress of 50 MPa. These steady state creep data are plotted against  $1/T$  in Fig. 4. From the slope of the line in Fig. 4, an apparent activation energy of  $700 \pm 25 \text{ kJ mol}^{-1}$  was determined.

#### 3.4. Microstructural observations

Transmission electron micrographs of the as-sintered material are shown in Figs 5a and b. The material is predominantly  $\beta\text{-Si}_3\text{N}_4$  with an average grain diameter of  $0.7 \mu\text{m}$ . The grain labelled A in Fig. 5a has an aspect ratio greater than 5. Equiaxed grain sizes up to approximately  $2.5 \mu\text{m}$  can be seen in Fig. 5a suggesting that some grain growth may have occurred during the sintering treatment. The silicon nitride grains are surrounded by a continuous glassy phase, which was shown by energy dispersive X-ray spectroscopy (EDX) to contain silicon and yttrium (dark region, labelled B in Fig. 5b).

Scanning electron micrographs of the specimen creep deformed for 1.5 h at 1673 K and an applied stress of 72.7 MPa are shown in Fig. 6. The polished,

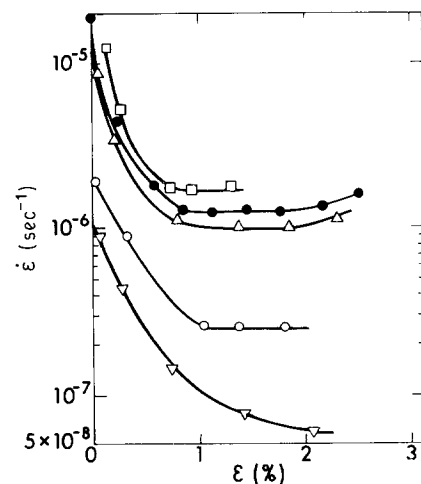


Figure 2 Creep strain rate,  $\dot{\epsilon}$ , plotted against strain,  $\epsilon$  (%) for specimens tested at 1673 K and applied stresses in the range 10.4 to 52 MPa ( $\nabla$  10.4,  $\circ$  19.9,  $\triangle$  39.1,  $\bullet$  41.6,  $\square$  52.0).

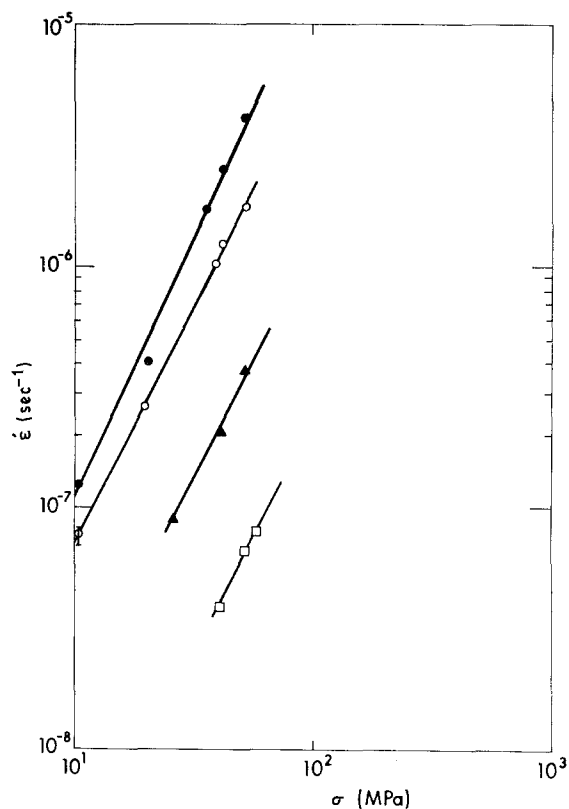


Figure 3 Steady state creep strain rate  $\dot{\epsilon}$  plotted against applied stress,  $\sigma$ , for temperatures of 1573 ( $\square$ ), 1623 ( $\blacktriangle$ ) and 1673K ( $\circ$ ,  $\bullet$ ) K.  $\bullet$  and  $\circ$   $\blacktriangle$   $\square$  represent specimens taken from different groups in the same batch process.  $n = 2.00 \pm 0.15$ .

unetched, tensile surface in Fig. 6a shows the development of cracks and cavities along boundaries perpendicular to the applied stress. Fig. 6b shows the thermally etched side of the specimen, adjacent to the fracture surface, with a region of incomplete sintering at the bottom right. The fracture surface, containing many small voids and cracks is shown in Figs 6c and d.

Transmission electron micrographs of the specimen creep tested for 22.4 h at 1673 K and a stress of 19.9 MPa are presented in Fig. 7. Evidence of grain boundary sliding (labelled A) and occasional dislocation activity (labelled B) can be seen in Fig. 7a. The glassy phase in Fig. 7a is seen to contain small ( $0.04 \mu\text{m}$ ) light areas in a dark matrix (labelled C). Tilting of the specimen did not reveal a change in contrast, indicating that these regions were not crystalline. Careful study of several regions, which were all found to be amorphous, and comparison of the micrographs with those of Leng-Ward and Lewis [28], suggested that the glass had separated into two amorphous phases during the creep test. Similar regions were only occasionally observed in the as-received specimen. It should be noted that there appeared to be evidence of phase separation immediately adjacent to the silicon nitride grains in several cases. An alternative explanation for the two phase regions might be the presence of gas bubbles, if the reduction of nitrogen ions to nitrogen gas were to occur at the  $\text{Si}_3\text{N}_4$ -glass interface.

Small crystalline regions, with only the elements silicon and yttrium being detected by EDX, were also observed in the creep tested sample. A more detailed study of the phases present is currently in progress,

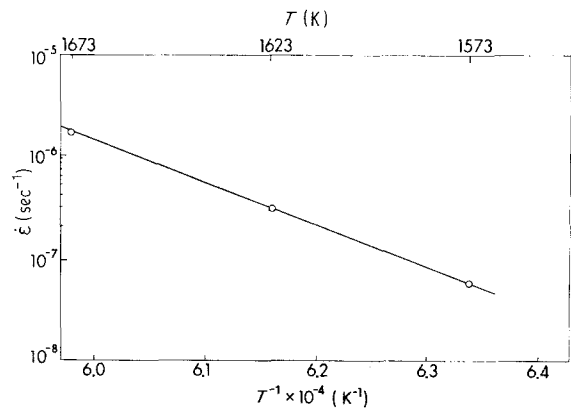


Figure 4 The variation in steady state creep strain rate with reciprocal temperature for  $\text{Si}_3\text{N}_4$ -6Y<sub>2</sub>O<sub>3</sub>-2Al<sub>2</sub>O<sub>3</sub> deformed at 50 MPa.  $Q = 700 \pm 25 \text{ kJ mol}^{-1}$ .

but it was clear that the majority of the grain boundary phase observed in the present study was amorphous.

The formation of creep cavities at triple points and deformation of the glassy phase are clearly seen in Fig. 7b. Meniscus formation can be seen at the regions labelled D in Fig. 7b.

### 3.5. X-ray diffraction data

X-ray diffraction data were taken from the specimen creep tested for 22.4 h at 1673 K and a stress of 19.9 MPa. These data confirmed the presence of  $\beta$ - $\text{Si}_3\text{N}_4$  with a trace of  $\alpha$ - $\text{Si}_3\text{N}_4$ , and X-ray lines could also be matched with yttrium aluminium garnet [ $1/2(3\text{Y}_2\text{O}_3 \cdot 5\text{Al}_2\text{O}_3)$ ]; aluminium yttrium oxides,  $\text{YAlO}_3$  and  $\text{Al}_5\text{Y}_3\text{O}_{12}$ ; and yttrium silicon oxide nitride,  $\text{Si}_3\text{N}_4 \cdot \text{Y}_2\text{O}_3$ . A detailed transmission electron microscopy study is now in progress to unambiguously identify the crystalline phases present.

### 3.6. Grain size measurements

Grain size measurements, from the transmission electron micrographs, were made for samples taken from the as-sintered material and the specimen crept at 19.9 MPa for 22.4 h at 1673 K. The average grain width increased from  $0.7 \pm 0.25 \mu\text{m}$  in the as-sintered material to  $1.0 \pm 0.25 \mu\text{m}$  in the crept material. There were insufficient data in the transmission electron micrographs to obtain accurate aspect ratio measurements. The limited data collected suggest that grain growth was not a major factor in the short term creep tests.

## 4. Discussion

### 4.1. Creep data

With the exception of the 10.4 MPa test at 1673 K, all the creep curves obtained for stresses above 19.9 MPa in the temperature range 1573 to 1673 K exhibited primary, secondary and tertiary creep regions. This is in agreement with (a) data reported by Heinrich and Böhmer [20] for four-point bend tests of hot isostatically pressed yttria-doped silicon nitride in air at 1623 K, and (b) other comprehensive studies of creep in hot pressed silicon nitride [1, 17, 29, 30]. In contrast, Arons and Tien [31] reported that for tensile creep tests of hot pressed silicon nitride containing magnesia additives (NC-132) no steady state creep was observed and the strain followed power law time kinetics. Similarly,

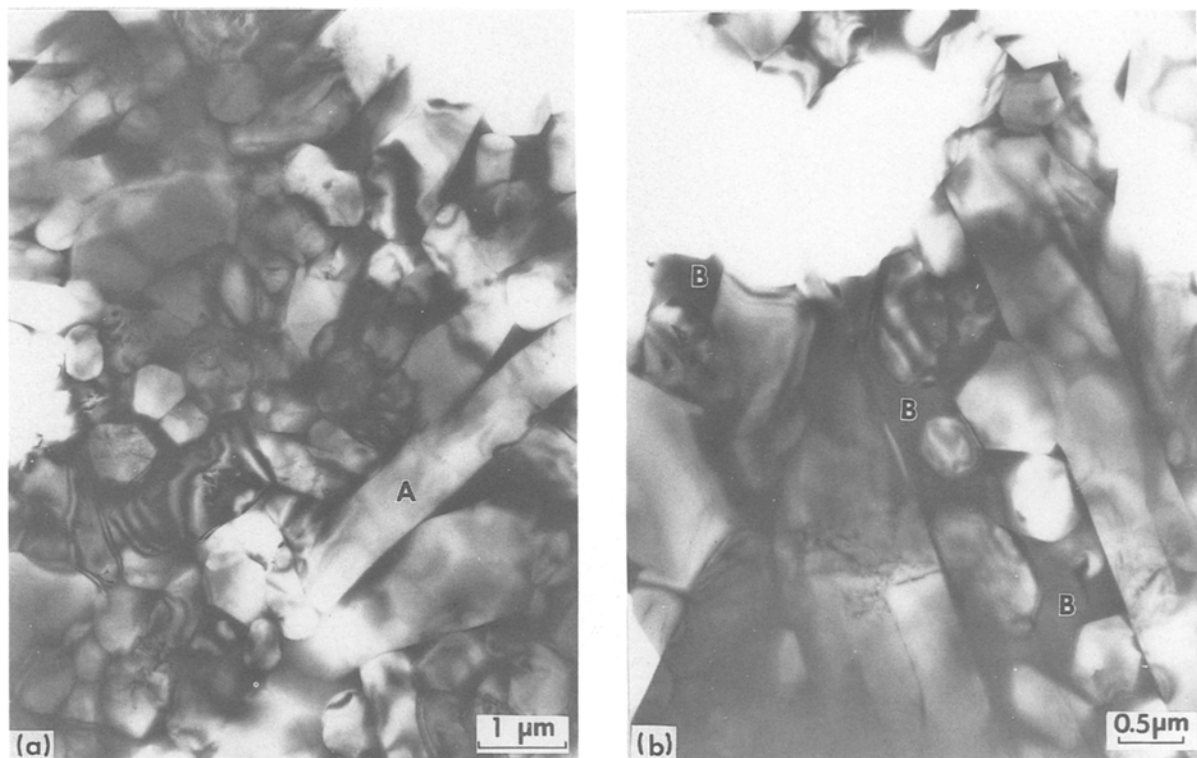


Figure 5 Transmission electron micrographs of the as-sintered  $\text{Si}_3\text{N}_4-6\text{Y}_2\text{O}_3-2\text{Al}_2\text{O}_3$ , (a) A –  $\beta\text{-Si}_3\text{N}_4$  grain with aspect ratio greater than 5, (b) B – continuous glassy phase surrounding silicon nitride grains.

Bouarroud *et al.*[25] reported a very long primary creep stage in creep tests of  $\text{Si}_3\text{N}_4-25\text{SiO}_2-5\text{Y}_2\text{O}_3$  (mol %). However, it should be noted that both Arons and Tien and Bouarroud *et al.* conducted their tests at lower temperatures (1450 to 1533 K) than the studies reported above (1573 to 1673 K). Their observations agree with those of Davies and Sinha-Ray [32], who noted that decreasing the test temperature increased the extent of primary creep in polycrystalline alumina.

#### 4.2. Stress exponent

The observations of deformation in the glassy phase at grain boundaries together with wedge cracks and cavitation suggests a viscoelastic mechanism, characterized by a stress exponent,  $n = 1$ . In the present study, a stress exponent of 2.0 was determined for  $\text{Si}_3\text{N}_4-6\text{Y}_2\text{O}_3-2\text{Al}_2\text{O}_3$  in agreement with data for SiAlON and silicon nitrides [17–19, 29–31, 33–42]. This apparent discrepancy has been reconciled by Evans and Rana [43], who have developed statistical models for the creep strain and the failure time of high temperature ceramics in the presence of grain boundary cavitation. Their model predicts a stress exponent of 2 for materials with a continuous grain boundary phase, in which cavities are formed by the viscous flow of the boundary phase in the presence of both an external stress and boundary sliding displacements.

#### 4.3. Activation energy for creep deformation

The steady state creep deformation of ceramic materials can be represented by an equation of the following form [23]

$$\dot{\epsilon} = \frac{AGbD}{kT} \left(\frac{b}{d}\right)^p \left(\frac{\sigma}{G}\right)^n \quad (1)$$

where,  $\dot{\epsilon}$  is the strain rate,  $G$  the shear modulus,  $b$  the Burger's vector,  $k$  the Boltzmann's constant,  $T$  the absolute temperature,  $D$  the diffusivity ( $=D_0 \exp[-Q/(RT)]$  with  $D_0$  constant),  $Q$  the activation energy of the appropriate diffusion process,  $R$  the gas constant,  $d$  the grain size,  $p$  the inverse grain size exponent,  $\sigma$  the applied stress and  $n$  the stress exponent.

The activation energy determined from the Arrhenius plot of strain rate against reciprocal temperature in Fig. 4 is given by the expression

$$Q_a = -R\partial \ln \dot{\epsilon}/\partial(1/T) \quad (2)$$

In order to identify the rate controlling mechanism, the true activation energy, given by the following expression, must be determined

$$Q_t = -R\partial \ln D/\partial(1/T) \quad (3)$$

Combining Equations 1 to 3 gives the following relationship between the true and apparent activation energies

$$Q_t = Q_a + RT - [(1 - n)RT^2/G]dG/dT \quad (4)$$

The shear modulus at temperature can be determined from the relationship

$$G_T = G_0 + (dG/dT)T \quad (5)$$

Shear modulus data as a function of temperature in air have been determined for silicon nitride by several authors [29, 44–47]. Kossowsky *et al.* [29], showed that the shear modulus varied linearly with temperature up to 1473 K, (giving a slope  $(dG/dT) = -8.97 \text{ MPa K}^{-1}$  and a value of  $G_0 = 1.24 \times 10^5 \text{ MPa}$ ) but decreased more rapidly above 1473 K. Similar values can be determined from the Young's modulus data

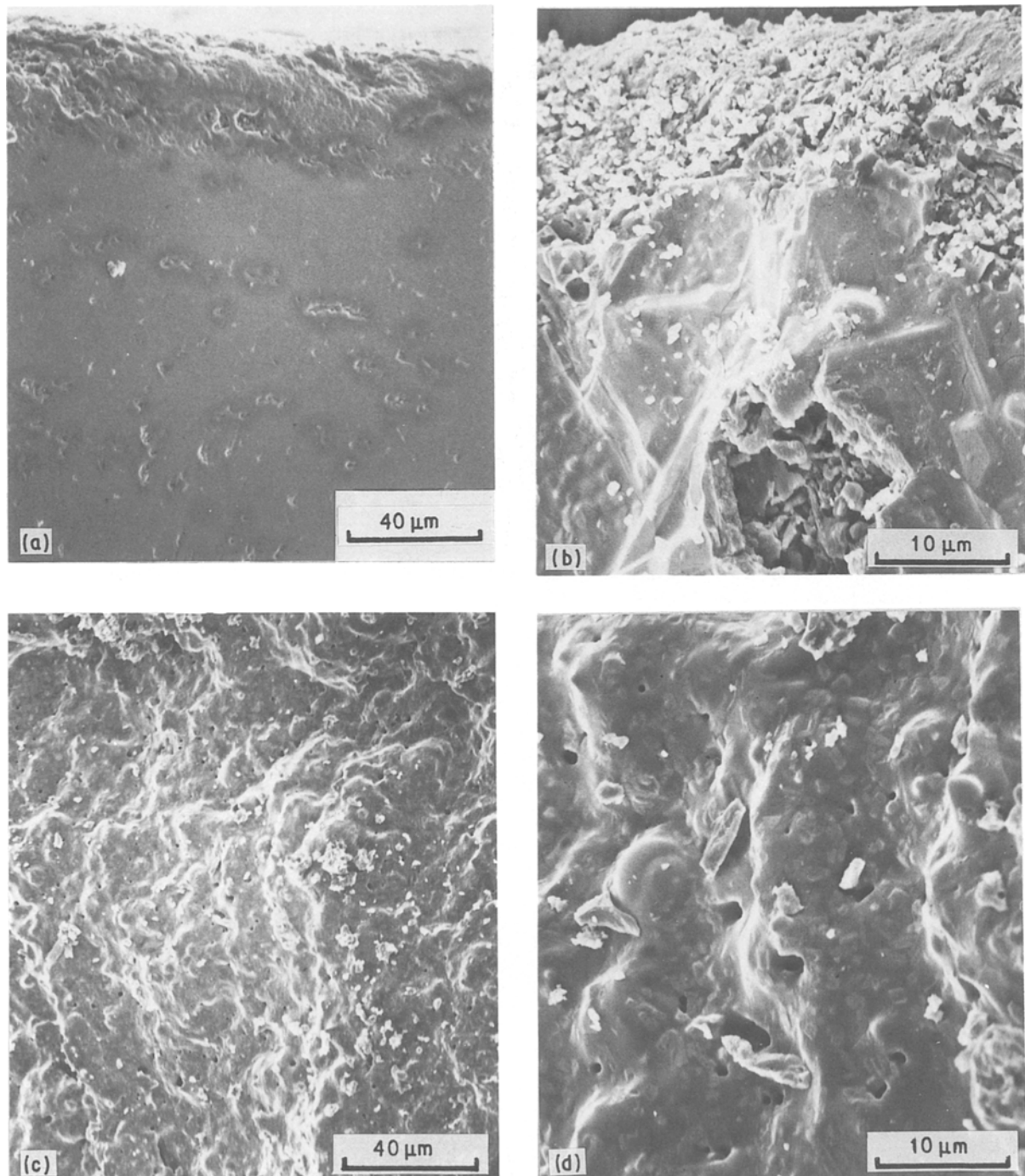


Figure 6 Scanning electron micrographs of specimen creep deformed for 1.5 h at 1673 K with an applied stress of 36.4 MPa, (a) polished, unetched tensile surface showing microcracks and cavities, (b) thermally etched side of the specimen showing region of incomplete sintering, (c) and (d) fracture surface showing small voids and cracks.

reported by Bonnell *et al.* for temperatures up to 1273 K (assuming  $\nu = 0.28$ ). Larsen and Adams [45] have reported a value of  $G = 1.3 \times 10^5$  MPa at 1748 K indicating that the linear extrapolation technique is an acceptable method for estimating the shear modulus in the temperature range 1573 to 1673 K. Using the extrapolated shear modulus data of Kosowsky *et al.*, a plot of  $\dot{\epsilon}G^{n-1}T$  against  $1/T$  was constructed giving a true activation energy of  $692 \pm 25$  kJ mol<sup>-1</sup>. This activation energy is in excellent agreement with activation energy data for silicon nitride, summarized in Table AIII of reference [23], with additional data in references [1, 20, 25].

#### 4.4. Identification of the rate controlling mechanism

The majority of the creep deformation studies of hot pressed, sintered, hot isostatically pressed and reaction bonded silicon nitride have determined the stress exponent,  $n$ , to be approximately 2, and the activation energy of the rate controlling mechanism to be in the range 600 to 750 kJ mol<sup>-1</sup>. Grain boundary sliding is observed in the amorphous grain boundary phase, accompanied by microcrack development [19, 29]. It has been suggested that deformation is strongly dependent on the viscosity of the grain boundary phase, the silicon nitride dissolution and reprecipitation reactions

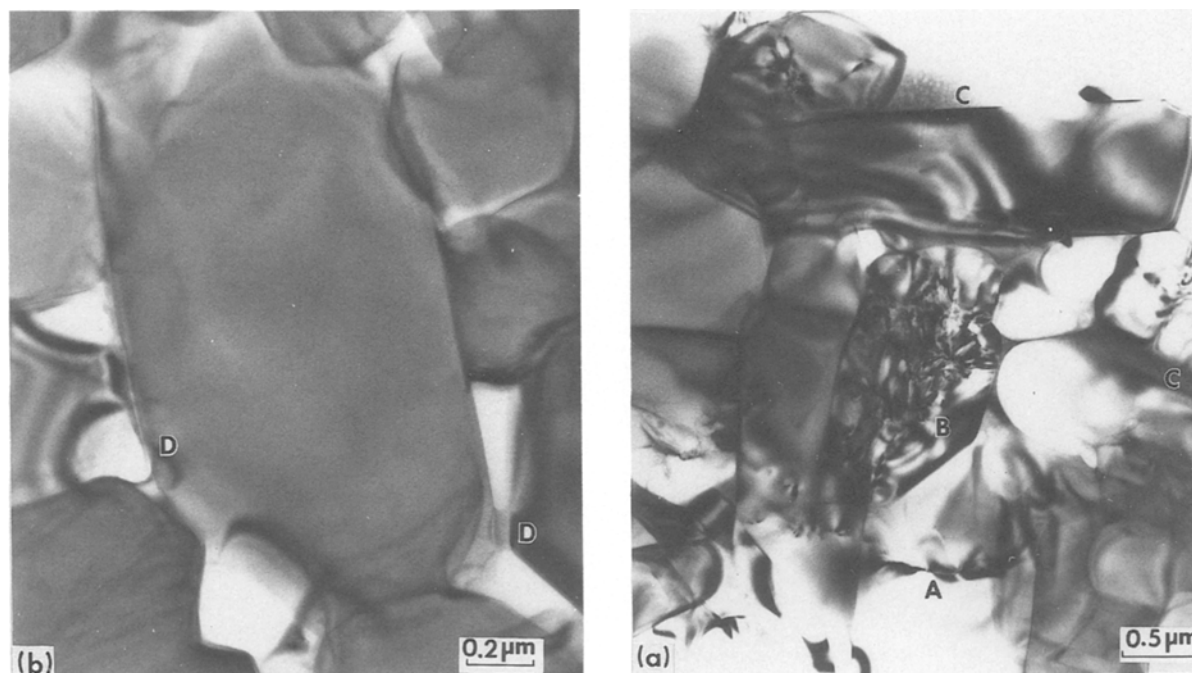


Figure 7 Transmission electron micrograph of specimen creep deformed for 22.4 h at 1673 K and a stress of 19.9 MPa. (a) A – grain boundary sliding, B – dislocation activity, C – phase separation within the glass. (b) Deformation in the glassy phase at grain boundaries, with meniscus formation at regions labelled D.

and the transfer of the viscous phase from boundaries under compression to those in tension [19, 29]. It is well established that additives such as CaO, which cause a marked reduction in the softening point and viscosity of silica glass, increase the creep strains and deformation rates of hot pressed silicon nitride [1, 17, 19, 29].

The existing creep data for silicon nitride fall into two groups: (a) data collected in the temperature range 1523 to 1673 K, where well defined steady state creep rates have been observed, as in the present study; and (b) data collected at lower temperatures 1373 to 1523 K, where only primary creep has been observed. Activation energies determined from the steady state data lie in the range 650 to 750 kJ mol<sup>-1</sup> and will now be compared with existing diffusion data for silicon nitride, and activation energies from primary creep and oxidation studies.

The self diffusion coefficients for nitrogen in single crystal grains of polycrystalline  $\alpha$ - and  $\beta$ -silicon nitride have been measured by Kijima and Shirasaki [48], giving values of 235 and 778 kJ mol<sup>-1</sup>, respectively. Although the value for  $\beta$ -Si<sub>3</sub>N<sub>4</sub> is only 78 kJ mol<sup>-1</sup> higher than the value of 700 kJ mol<sup>-1</sup>, measured in the present study, it is unlikely that bulk diffusion of nitrogen would be rate controlling in the presence of a continuous, amorphous grain boundary phase. However, very limited diffusion data are available for these grain boundary phases. Wötting [1, 49] reports values for Si–N diffusion in the grain boundary phase of hot pressed silicon nitride of (a) 448 kJ mol<sup>-1</sup> at temperatures below 1823 K and (b) 695 kJ mol<sup>-1</sup> at temperatures above 1823 K (for 10 wt % Y<sub>2</sub>O<sub>3</sub> additive); and (c) 645 kJ mol<sup>-1</sup> (for 5 wt % MgO additive–temperature range not indicated).

The primary creep studies give a wider range of

activation energy values. Arons and Tien [31], in agreement with Lange *et al.* [41], concluded that permanent creep and viscoelastic deformation were parallel processes which could be treated independently. Activation energies of 403 ± 113 kJ mol<sup>-1</sup> (at constant strain (0.9%)) and 848 kJ mol<sup>-1</sup> (at constant time (10 h)), were determined by Arons and Tien for three-point bend tests of NC-132 (MgO additive) in the temperature range 1450 to 1533 K. Tests at constant structure were carried out by temperature jump experiments on a single specimen with significant creep strain, giving an activation energy of 819 ± 84 kJ mol<sup>-1</sup>, which confirmed the value of 848 kJ mol<sup>-1</sup> determined above. The activation energy for the viscoelastic process was obtained through the temperature dependence of the recovery rate (taken 4 h after load removal) and was found to be 722 kJ mol<sup>-1</sup>. Arons and Tien concluded that the persistent creep deformation occurred by grain boundary sliding accommodated by grain boundary phase percolation and cavitation void and wedge opening.

A study of both primary creep and the oxidation kinetics of 70Si<sub>3</sub>N<sub>4</sub>–25SiO<sub>2</sub>–5Y<sub>2</sub>O<sub>3</sub> (mol %) has been conducted by Bouarroud *et al.* [25]. They showed that oxidation occurred in the intergranular glass phase with activation energies of 146 ± 15 and 680 ± 80 kJ mol<sup>-1</sup>, for the temperature ranges 1453 to 1693 K and 1693 to 1923 K, respectively. In the lower temperature regime, they suggested that the inward diffusion of oxygen could be the limiting step, whereas at higher temperatures, the outward diffusion of an “yttrium–nitrogen” compound species was thought to be the limiting step. The oxidation data were related to the creep data by using the strain rates at constant degree of oxidation (i.e. constant weight gain) to determine the activation energy. It should be noted

that no grain growth was observed in this material. Irrespective of the weight gain value selected, an activation energy of 720 kJ mol<sup>-1</sup> was determined. This value is identical to that determined by Tien for the viscoelastic process and is very close to the value of 700 kJ mol<sup>-1</sup> measured in the present study.

Bouarroud *et al.* modelled the primary creep strain,  $\varepsilon$ , as the sum of the viscoelastic component,  $\varepsilon_v$ , and the diffusional component,  $\varepsilon_d$ , giving

$$\varepsilon = \varepsilon_v + \varepsilon_d \quad (6)$$

and

$$\dot{\varepsilon} = \dot{\varepsilon}_v + \dot{\varepsilon}_d \quad (7)$$

From the analysis of Lange *et al.* [41], the creep rate was written as

$$\dot{\varepsilon} = \frac{1}{\eta} f(S_v, \sigma) + S_d \sigma \exp(-E_d/RT) \quad (8)$$

where  $\eta$  is the viscosity of the grain boundary phase;  $S_v$  depends on the structural state of the material ( $S_v(S_0, D, E, A)$  where  $S_0$  is the thickness of the glassy interphase,  $D$  the mean grain size;  $E$  the elastic modulus of a grain boundary asperity;  $A$  the areas of the asperity)  $\sigma$  the applied stress,  $S_d$  depends on the structural state and  $E_d$  is the activation energy of the diffusional mechanism.

An Arrhenius expression was assumed for the viscosity giving

$$\dot{\varepsilon} = \frac{1}{\eta_0} f(S_v, \sigma) \exp(-E_v/RT) + S_d \sigma \exp(-E_d/RT) \quad (9)$$

where  $E_v$  is the activation energy of the glass viscosity.

The experimental observation that the activation energy measured was constant for all weight gains, led Bouarroud *et al.* to the conclusion that  $E_v$  must be equal to  $E_d$  and that matter transport through the glassy phase was the rate limiting step.

#### 4.5. Relationship between the viscosity and diffusivity of a liquid

The above conclusion can be reconciled with the activation energy values obtained by (a) Arons and Tien, (b) in the present study, and (c) in silicon nitride containing magnesia or yttria additives, when the Einstein relationship between the mobility of a liquid and its diffusivity is introduced [50].

The resistance,  $F$ , suffered by a small sphere of liquid of radius  $a$ , moving with an average velocity,  $\bar{v}$ , with respect to the surrounding particles is given by Stokes' law

$$F = 6\pi a \eta \bar{v} \quad (10)$$

This can be written as

$$\bar{v} = \alpha F \quad (11)$$

where  $\alpha$  is the mobility of the particle, given by

$$\alpha = \frac{1}{6\pi a \eta} \quad (12)$$

According to Einstein's theory of Brownian motion

$$\alpha = \frac{D}{kT} \quad (13)$$

where  $D$  is the self diffusion coefficient of the liquid,  $k$  the Boltzmann's constant and  $T$  the temperature (K). Hence

$$\eta = \frac{kT}{6\pi a D} \quad (14)$$

and if

$$D = D_0 \exp(-E'_d/kT) \quad (15)$$

where  $E'_d$  is equivalent to  $E_d$  in Equation 9

$$\eta = \frac{kT}{6\pi a D_0} \exp(E'_d/kT) \quad (16)$$

showing that the activation energy for the viscosity is the same as that for the self diffusion of the liquid.

The kinetic theory for the viscosity of liquids was developed by Frenkel in 1926 [51] and is discussed in detail in reference [52].

#### 4.6. The role of additives

In deriving the relationship between the viscosity and self diffusivity of a liquid (Equation 16), Frenkel assumed that the average resistance of the liquid to the motion of one of its particles could be determined by Stokes law [39]. If a particle of the liquid is replaced by a particle of a foreign substance dissolved in the liquid, then by Stokes law, there will be very little change in the mobility for the foreign particle unless there is a large difference in the radii of the particles. Hence the diffusion coefficients of the different dissolved species must be approximately equal to each other and to the self-diffusion coefficient of the solvent.

This concept can be applied to silicate glasses by assuming that the various "particle sizes" are associated with the silica tetrahedra and the diffusing ions. The circumscribed sphere for the silica tetrahedron has a radius of 0.152 nm compared to the following radii for the respective ions: 0.171 nm N<sup>3-</sup>; 0.14 nm O<sup>2-</sup>; 0.065 nm Mg<sup>2+</sup>; 0.099 nm Ca<sup>2+</sup>; 0.05 nm Al<sup>3+</sup>; 0.093 nm Y<sup>3+</sup>; 0.041 nm Si<sup>4+</sup>. It should be noted that the circumscribed sphere for the silica tetrahedron was determined using the ionic radii modified by the coordinate number (CN), i.e. O<sup>2-</sup> = 0.114 nm (CN 2) and Si<sup>4+</sup> = 0.038 (CN 4) [53–56]. Hence, there is little difference between the radii of the diffusing species, with the radius of the nitrogen ion, N<sup>3-</sup>, being the largest. This result suggests that the diffusion of the nitrogen ion may be the rate controlling mechanism, as discussed below in the context of the oxidation mechanism.

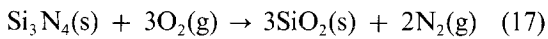
The correlation between viscosity and diffusivity has been investigated by Schaeffer for vitreous silica [57–59]. He concluded that the diffusivity of silicon or the SiO<sub>4</sub> tetrahedron was rate controlling for viscous flow phenomena involving the silica phase, such as the high temperature creep of ceramic materials with silica-rich grain boundaries. However, he noted that the oxidation data of Si<sub>3</sub>N<sub>4</sub> differed from those for Si, MoSi<sub>2</sub> and SiC and suggested that the release of



nitrogen at the  $\text{Si}_3\text{N}_4\text{-SiO}_2$  interface may be responsible. Further research is now required to determine whether the two-phase regions observed in the glass phase of  $\text{Si}_3\text{N}_4\text{-6Y}_2\text{O}_3\text{-2Al}_2\text{O}_3$  correspond to the presence of (a) nitrogen-rich glass; (b) oxygen-rich glass; or (c) nitrogen gas bubbles; in order to clarify the rate controlling mechanism.

#### 4.7. Relationship between the creep mechanism and oxidation

When silicon nitride is creep tested in air, passive oxidation, at high oxygen levels in the atmosphere, results in a protective  $\text{SiO}_2$  rich layer forming at the surface, according to the reaction



In magnesia-fluxed materials it has been shown that the chemical potential gradient established results in an increase of the magnesium ion concentration in the surface scale. Diffusion of the magnesium cations from the bulk to the surface was proposed as the rate controlling mechanism for oxidation [60, 61]. Similarly, Bouarroud *et al.* [25] reported segregation of yttrium to the subscale during oxidation of  $70\text{Si}_3\text{N}_4\text{-25SiO}_2\text{-5Y}_2\text{O}_3$ , but concluded that the limiting step was matter transport through the glassy grain boundary phase, possibly by an "yttrium-nitrogen compound" (complex).

In the present work, we conclude that the rate limiting step may be the transport of the nitrogen ions, rather than a complex species, through the grain boundary glassy phase to the surface as illustrated schematically in Fig. 8. The silicon nitride grains are shown surrounded by the glassy phase and exposed to air. At the surface, nitrogen ions in the glass give up electrons and form nitrogen gas. This reaction can only occur if there is a species in the glass or the surrounding environment to accept the electrons. In this case oxygen atoms accept electrons, forming ions, with  $6\text{O}^{2-}$  ions being formed for every  $4\text{N}^{3-}$  converted to nitrogen gas. The oxygen anions will attach to available network cations, and once these are exhausted will induce a flux of cations from the bulk to the

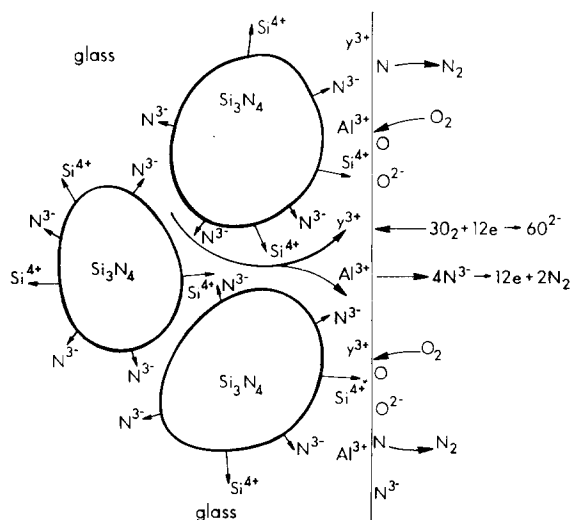


Figure 8 Schematic representation of the oxidation and reduction reactions accompanying the creep deformation of  $\text{Si}_3\text{N}_4\text{-6Y}_2\text{O}_3\text{-2Al}_2\text{O}_3$  when tested in air.

surface. This flux will include the cations in the glass, e.g.  $\text{Y}^{3+}$ ,  $\text{Mg}^{2+}$ ,  $\text{Al}^{3+}$  and also  $\text{Si}^{4+}$  ions from the dissolution of the silicon nitride. A parallel flux of nitrogen anions to the surface, also from the dissolution of the silicon nitride, will occur to replace the nitrogen ions evolved as nitrogen gas. Since  $\text{N}^{3-}$  has the largest ionic radius it is likely to have the slowest diffusivity, resulting in nitrogen ion transport through the glassy phase being the rate limiting step.

#### 4.8. Interpretation of creep data

The above mechanistic interpretation can provide a satisfactory explanation for much of the creep data available for silicon nitride.

(1) The activation energies measured for creep of silicon nitride fall within the range  $600$  to  $750 \text{ kJ mol}^{-1}$  irrespective of the type of additive, since nitrogen transport is the rate limiting step in each case.

(2) The creep mechanism is identical for the primary and steady state studies described above for the temperature ranges  $1373$  to  $1523 \text{ K}$  and  $1523$  to  $1673 \text{ K}$ , with the true steady state being reached when there is a constant flux of  $\text{N}^{3-}$  ions from the bulk to the surface.

(3) The creep rates of silicon nitride are much lower in helium environments since there is no surface species (e.g.  $\text{O}_2$ ) to accept electrons, and the concentration of impurities, such as  $\text{Fe}^{3+}$ , which could change oxidation state is generally very low [29].

(4) The viscosity of the glass increases with time, i.e. a hardening effect is observed during long term creep tests. This could be attributed to increasing nitrogen concentration levels in the oxynitride glass, rather than to the depletion of  $\text{Mg}^{2+}$  or  $\text{Y}^{3+}$ . For example, Drew *et al.* [62] have established a correlation between increasing viscosity and increasing nitrogen levels in a series of oxynitride glasses of constant metal atom context.

(5) Once crystallization of the glassy phase occurs, matter transport through the crystalline regions will become important, and the activation energy and rate limiting mechanism for the creep process must change. Activation energies may change continuously with temperature reflecting the increased degree of crystallization in the grain boundary phase.

(6) The strain rate derived by Evans and Rana [43] for a material with a continuous grain boundary phase

$$\dot{\epsilon} = \omega \sigma_{\infty}^2 E^{-1} \exp(-Q_{\eta}/RT) \quad (18)$$

(where  $\omega$  is a constant,  $\sigma_{\infty}$  the remote stress,  $E$  the Young's modulus and  $Q_{\eta}$  the activation energy for the viscous mechanism) can now be replaced by

$$\dot{\epsilon} = \omega' \sigma_{\infty}^2 E^{-1} \exp(-Q_D/RT) \quad (19)$$

where  $\omega'$  is a constant and  $Q_D$  the activation energy for diffusion through the grain boundary phase.

Hence creep can be shown to occur by a diffusion controlled mechanism with a stress exponent,  $n = 2$ .

## 5. Conclusions

The conclusions are as follows.

(1) The creep properties of  $\text{Si}_3\text{N}_4\text{-6Y}_2\text{O}_3\text{-2Al}_2\text{O}_3$ ,



prepared by a two-stage gas pressure sintering process, have been determined in the temperature range 1573 to 1673 K, giving a stress exponent,  $n = 2.00 \pm 0.15$  and a true activation energy of  $692 \pm 25 \text{ kJ mol}^{-1}$ .

(2) The creep exponent,  $n = 2$ , can be rationalized in terms of Newtonian viscous sliding accompanied by microcrack formation and cavitation.

(3) The viscosity of the grain boundary phase has the same activation energy as that for the self diffusion of the liquid, when Einstein's relationship between the mobility and the diffusivity of a liquid is introduced.

(4) The activation energy is consistent with a diffusion controlled mechanism, with the rate controlling mechanism being the transport of nitrogen ions through the grain boundary phase.

(5) The mechanistic interpretation proposed provides an explanation for the role of (a) additives; (b) helium environments; (c) observed viscosity changes; and (d) crystallization, during the creep testing of silicon nitride ceramics.

### Acknowledgements

This research was supported by the National Aeronautics and Space Administration under grant number NASA NAG 3-685. The authors would like to thank the AiResearch Casting Company of the Garrett Corporation for supplying the material; Dr Hun Yeh of the AiResearch Casting Company and Dr A. Chokshi, U. C. Davies, for many helpful discussions during this research; and Karrel de la Cruz for assistance with the creep tests. Zhi-Yue Xu was supported as a visiting scholar by the South-West Petroleum Institute, Peoples' Republic of China, and by the National Oceanic and Atmospheric Agency through the USC Sea Grant Program. This research was funded in part by (a) an appointment (J. A. Todd) to the U.S. Department of Energy Faculty Research Participation Program (1986) administered by Oak Ridge Associated Universities; and (b) the Basic Energy Sciences Division, USDOE, through the SHaRE program under contract DE-AC05-76ORO0033 with Oak Ridge Associated Universities. The authors gratefully acknowledge all the above support.

### References

1. G. ZIEGLER, J. HEINRICH and G. WÖTTING, *J. Mater. Sci.* **22** (1987) 3041.
2. G. G. DEELY, J. M. HERBERT and N. C. MOORE, *Powder Metall.* **8** (1961) 145.
3. Y. OYAMA and O. KAMIGAITO, *Jpn J. Appl. Phys.* **10** (1971) 1637.
4. G. E. GAZZA, *J. Amer. Ceram. Soc.* **56** (1973) 662.
5. I. C. HUSEBY and G. PETZOW, *Powder Met. Int.* **6** (1974) 17.
6. H. HAUSNER, *Sci. Ceram.* **12** (1983) 229.
7. K. S. MAZDIYASNI and C. M. COOKE, *J. Amer. Ceram. Soc.* **57** (1974) 536.
8. S. H. KNICKERBOCKER, A. ZANGVIL and S. D. BROWN, *ibid.* **68** (1985) C99.
9. D. R. CLARKE and G. THOMAS, *ibid.* **60** (1977) 491.
10. O. L. KRIVANEK, T. M. SHAW and G. THOMAS, *ibid.* **62** (1979) 585.
11. L. K. V. LOU, T. E. MITCHELL and A. H. HEUER, *ibid.* **61** (1978) 392.
12. A. TSUGE and K. NISHIDA, *ibid.* **58** (1975) 323.
13. *Idem*, *Amer. Ceram. Soc. Bull.* **57** (1978) 424.

14. D. R. CLARKE and G. THOMAS, *J. Amer. Ceram. Soc.* **61** (1978) 114.
15. C. C. AHN and G. THOMAS, *ibid.* **66** (1983) 14.
16. F. F. LANGE, *Int. Met. Rev.* **1** (1980) 1.
17. S. UD DIN and P. S. NICHOLSON, *J. Mater. Sci.* **10** (1975) 1375.
18. J. M. BIRCH and B. WILSHIRE, *ibid.* **13** (1978) 2627.
19. P. J. DIXON-STUBBS and B. WILSHIRE, *ibid.* **14** (1979) 2773.
20. J. HEINRICH and M. BÖHMER, *Ber. Dtsch Keram. Ges.* **61** (1984) 399.
21. C. L. QUACKENBUSCH, J. T. SMITH, J. T. NEIL and K. W. FRENCH, in "Progress in Nitrogen Ceramics", edited by F. L. Riley (Martinus-Nijhoff, Dordrecht, 1983) p. 669.
22. L. J. BOWEN, T. J. CARRUTHERS and R. J. BROOK, *J. Amer. Ceram. Soc.* **61** (1978) 335.
23. W. R. CANNON and T. G. LANGDON, *J. Mater. Sci.* **18** (1983) 1.
24. *Idem*, *ibid.* **23** (1988) 1.
25. A. BOUARROUD, J. P. GOURSAT and J. L. BESSON, *ibid.* **20** (1985) 1150.
26. G. Q. WEAVER and J. W. LUCEK, *Amer. Ceram. Soc. Bull.* **57** (1978) 1131.
27. G. W. HOLLENBERG, G. R. TERWILLIGER and R. S. GORDON, *J. Amer. Ceram. Soc.* **54** (1971) 196.
28. G. LENG-WARD and M. H. LEWIS, *Mater. Sci. Engng* **71** (1985) 101.
29. R. KOSSOWSKY, D. G. MILLER and E. S. DIAZ, *J. Mater. Sci.* **10** (1975) 983.
30. M. S. SELTZER, *Ceram. Bull.* **56** (1977) 418.
31. R. M. ARONS and J. K. TIEN, *J. Mater. Sci.* **15** (1980) 2046.
32. C. K. L. DAVIES and S. K. SINHA RAY, in "Special Ceramics", edited by P. Popper (British Ceramic Research Association, Stoke-on-Trent, 1972), p. 193.
33. R. KOSSOWSKY, in "Ceramics for High-Performance Applications", edited by J. J. Burke, A. E. Gorum and R. N. Katz (Brook Hill, Chestnut Hill, Massachusetts, 1974), p. 347.
34. J. A. MANGELS, *ibid.* p. 195.
35. W. ENGEL, E. GUGEL and F. THÜMMLER, in "Science of Ceramics", Vol. 7 (Société Francaise de Céramique, Paris, 1976) p. 415.
36. J. M. BIRCH, B. WILSHIRE, D. J. R. OWEN and D. SHANTARAM, *J. Mater. Sci.* **11** (1976) 1817.
37. J. M. BIRCH, B. WILSHIRE and D. J. GODFREY, *Proc. Brit. Ceram. Soc.* **26** (1978) 141.
38. G. GRATHWOHL and F. THÜMMLER, *J. Mater. Sci.* **13** (1978) 1177.
39. P. K. TALTY and R. A. DIRKS, *ibid.* **13** (1978) 580.
40. G. GRATHWOHL and F. THÜMMLER, *Ceramurgia Int.* **6** (1980) 43.
41. F. F. LANGE, B. I. DAVIS and D. R. CLARKE, *J. Mater. Sci.* **15** (1980) 601.
42. J. A. PALM and C. D. GRESKOVICH, *Bull. Amer. Ceram. Soc.* **59** (1980) 447.
43. A. G. EVANS and A. RANA, *Acta Metall.* **28** (1980) 129.
44. D. A. BONNELL, T. Y. TIEN, M. LEE and M. K. BRUN, in 2nd International Conference Science Hard Materials (*Inst. Phys. Conf. Ser.* No. 75) (Adam Hilger, Bristol, 1986) p. 401.
45. D. C. LARSEN and J. W. ADAMS, "Property Screening and Evaluation of Ceramic Turbine Materials"; Semiannual Report No. 8, June, 1980, USAF Contract F33615-C-5100, pp. 22, 55.
46. R. R. WILLS, R. W. STEWART and J. M. WIMMER, *Ceram. Bull.* **56** (1977) 194.
47. W. A. FATE, *J. Amer. Ceram. Soc.* **57** (1974) 49.
48. K. KIJIMA and S. SHIRASAKI, *J. Chem. Phys.* **65** (1976) 2668.
49. G. WÖTTING, Thesis, TU Berlin (1983).
50. A. EINSTEIN, *Ann. Phys.* **19** (1905) 371.
51. J. FRENKEL, *Z. Phys.* **35** (1926) 652.
52. *Idem*, "Kinetic Theory of Liquids" (Dover, New York, 1955) p. 191.

53. L. H. VAN VLACK, "Elements of Materials Science and Engineering", 5th Edn (Addison Wesley, Reading, Massachusetts, 1985) p. 48.
54. A. R. WEST, "Solid State Chemistry and its Applications" (John Wiley, New York, 1984) p. 271.
55. R. D. SHANNON and C. T. PREWITT, *Acta Crystallogr.* **B25** (1969) 725.
56. *Idem, ibid.* **B26** (1970) 1046.
57. H. A. SCHAEFFER, "Encyclopedia of Materials Science and Engineering", edited by M. B. Bever (Pergamon, New York, 1986) p. 4396.
58. H. A. SCHAEFFER, *J. Non-Cryst. Solids* **38/39** (1980) 545.
59. *Idem, ibid.* **67** (1984) 19.
60. D. R. CLARKE, in "Progress in Nitrogen Ceramics", edited by F. L. Riley (Martinus-Nijhoff, Dordrecht, 1983) p. 421.
61. P. VINCENZINI and A. BABINI, in "Sintered Metal-Ceramic Composites", edited by G. S. Upadhyaya (Elsevier, Amsterdam, 1984) p. 425.
62. R. DREW, S. HAMPSHIRE and K. H. JACK, in "Progress in Nitrogen Ceramics", edited by F. L. Riley (Martinus-Nijhoff, Dordrecht, 1983) p. 323.

*Received 19 September 1988  
and accepted 24 February 1989*